Fatigue life extension of existing welded structures via high frequency mechanical impact (HFMI) treatment

Engineering Structures 239 (2021) 112234

Contents lists available at ScienceDirect

Engineering Structures

journal homepage: www.elsevier.com/locate/engstruct

Fatigue life extension of existing welded structures via high frequency mechanical impact (HFMI) treatment

Hassan Al-Karawi [a,*], Rüdiger U. Franz von Bock und Polach [b], Mohammad Al-Emrani [a]

[a] Architecture and Civil Engineering Department, Chalmers University of Technology, Gothenburg, Sweden
[b] Institute for Ship Structural Design and Analysis, Hamburg University of Technology, Hamburg, Germany

ARTICLE INFO

Keywords:
Existing structures
Steel bridges
High frequency mechanical impact
Fatigue life extension
Pre-fatigue
Crack repair

ABSTRACT

High Frequency Mechanical Impact (HFMI) is one of the post-weld treatment methods. In this study, comparative axial fatigue tests were conducted on as-welded and HFMI-treated welded transverse attachment details. The test results demonstrated the efficiency of HFMI-treatment in fatigue life extension of cracked welded structures, providing that the existing crack size is less than 1.2 mm. Cracks were created in some specimens through fatigue testing before HFMI-treatment, while other specimens were not subjected to any fatigue loading prior to treatment. Many of the treated specimens ran-out after 10 million cycles of loading when tested at a stress range of 150 MPa. Therefore, the stress range was increased to 180 MPa or 210 MPa. No remarkable difference was found between the fatigue strength of the crack-free and the cracked treated specimens. It was found that the induced compressive residual stress can exceed the material yield limit, and reach a depth larger than 1.5 mm in most of the cases. The induced compressive residual stress, the local material hardening, the increase in weld toe radius, the change in crack orientation and the shallowness of the crack size were the causatives of the obtained long fatigue lives of the HFMI-treated specimens. Besides, linear elastic fracture mechanics calculations were conducted to predict the fatigue lives of as-welded and HFMI-treated details. The results were in agreement with the experiment. Moreover, the calculations showed that the initial crack size, the clamping stress and the induced compressive residual stress were the main factors behind the scatter in fatigue lives.

1. Introduction

Many welded bridges in Europe were constructed in the few decades following the second world war. Thereby, there is a persistent need for maintaining their structural integrity. Fatigue process occurs over time and under loads lower than the ultimate limit state [1]. The degradation of the structure's integrity with time is -mainly- attributed to the vulnerability of welded joints to fatigue cracks when subjected to cyclic loading. Therefore, fatigue of welds gained increasing attention among researchers in structural engineering. Particularity when the design fatigue life has been reached and a decision is to be made whether the structure should be torn down and replaced or repair action could be sufficient to maintain the structure's integrity.

The vulnerability of welds to fatigue damage is traced back to several reasons: the tensile welding residual stress, the high stress concentration factor and the intrinsic weld defects (e.g. undercut) are the main ones. On the other hand, when the structure is cracked, the size of the crack appears to be one of the most prominent factors limiting the fatigue life [2]. Several post-weld treatment methods have been proposed in the literature which can be classified into two groups: the first comprises the residual stress changers (e.g. peening and stress relief), while the second group contains the topography improvers (e.g. grinding and TIG-dressing) [3].

High frequency mechanical impact (HFMI) is a relatively cheap weld treatment method. This method is known by different terms in the literature: hammer peening, ultrasonic impact treatment, ultrasonic needle peening and high frequency impact treatment (HiFIT). One of the main beneficial effects of HFMI-treatment is the increase of local compressive residual stress. In addition to that, it also reduces the notch effect and increases the local hardness. In comparison to other traditional HFMI-treatment techniques, HiFIT is more user-friendly, safer, easier to operate and produces finer surface finish because of the smaller

* Corresponding author at: Chalmers University of Technology, Department of Architecture and Civil Engineering, Research Group, Lightweight Structures, 41296 Göteborg, Sweden.
E-mail addresses: hassan.alkarawi@chalmers.se (H. Al-Karawi), franz.vonbock@tuhh.de (R.U.F. von Bock und Polach), Mohammad.Al-Emrani@chalmers.se (M. Al-Emrani).

https://doi.org/10.1016/j.engstruct.2021.112234
Received 2 October 2020; Received in revised form 26 January 2021; Accepted 8 March 2021
Available online 9 April 2021

spacing between the alternate impacts [4].

The efficiency of HFMI-treatment depends on many factors such as the indentor's radius, the acceleration of the treatment, the number of indentors, the applied load levels, the treated steel quality, the treated geometry and the existing crack size. The indentor's radius, the number of indentors and the treatment acceleration affect the geometry of the treated details and determine the local toe radius and the indentation depth [5]. Furthermore, HFMI-induced compressive residual stresses are larger for materials with higher yield strength [6]. Besides, since HFMI is a surface treatment method, its efficiency is limited by the existing crack size [7].

In fatigue assessment, 'pre-fatigue loading' indicates that a structure has been subjected to cyclic stresses prior to the application of HFMI-treatment [8]. This parameter can be introduced in fatigue testing by two methods. In the first one, the effect of loading before treatment is represented by the number of cycles and the applied stress level. The benefit of using this kind of representation is the simplicity and ease of application in the laboratory. However, the number of cycles before treatment is not always known in bridges. Günter et al. [9] found that treating transverse attachments by ultrasonic impact indentor after pre-fatigue loading of 75–90% of the estimated as-welded fatigue life caused a life prolongation by a factor of 2.5. Kudryavtsev et al. [10] concluded that fatigue strength of treated prefatigued specimens was higher than the fatigue strength of the treated virgin ones. However, Zhang et al. [11] found that the efficiency of peening decreases as a function of the prefatigue number of cycles.

Another way of representing the loading history in the laboratory is to pre-fatigue the structure until a crack is detected at the weld toe. This methodology was followed in [7,8,12–14]. Leitner et al. [8] studied the effect of HFMI-treatment on cracked longitudinal attachment and recommended not to apply this treatment when the crack is deeper than 0.5 mm. On the other hand, Branco et al. [7] & Fisher et al. [13,14] concluded that HFMI can treat cracks up to 2.5 and 3 mm deep respectively. Maddox et al. [12] found that fatigue crack could start from the weld root after HFMI-treatment because of the significant strength enhancement at the weld toe.

Instead of generating the cracks by fatigue loading, Houjou et al. [2] & Fueki et al. [15,16] created artificial cracks to represent the prefatigue loading stage. They concluded that HFMI-treatment efficiency decreases as the crack size increases. There is no consensus on the maximum allowable crack size which can be repaired by HFMI-treatment. This is attributed to the variabilities in crack detection methods, retrofitting depths, applied load levels and compressive residual stresses. Nonetheless, Al-Karawi & Al-Emrani [3] conducted a literature study and recommended that 2.25 mm crack is the maximum allowable crack size before HFMI-treatment.

The crack behaviour after HFMI-treatment has been studied in some articles [11,17–19]. Zhang et al. [11] investigated the fractography surfaces of HFMI-treated cracked and crack-free specimens. In the latter case, stamp-like impressions were found at the weld toe. Parallel plastic deformations caused by compressing the existing crack were found in the former case. Besides, several finite element analyses were conducted to study the effect of crack size on HFMI-treatment efficiency. It was concluded that the mechanism of improving the fatigue performance by peening is a function of the compressive residual stress, the crack size and the change in crack orientation. Zhiyuan et al. [17,18] observed that the crack opening is an important factor in determining HFMI-treatment efficiency. It was also found that the plastic deformations of the cracked surfaces were three times larger than the un-cracked ones. Al-Karawi et al. [19] conducted metallographic and numerical analyses and concluded that HFMI-treatment caused a change in crack orientation, a crack closure and induced compressive plasticity at the crack tip.

Linear elastic fracture mechanics (LEFM) can be used as a tool for fatigue life assessment. Leitner et al. [8] employed both weight function and parametric approaches to estimate the fatigue life of HFMI-treated longitudinal attachment. Branco et al. [7] used Paris law to estimate the gain factor in fatigue life after hammer peening. However, the results were not satisfactory because the effect of residual stress was not incorporated [20]. Fueki et al. [15,16] introduced a qualitative assessment based on the threshold stress intensity factor (K_{th}). More details on the use of LEFM in assessing HFMI-treatment in cracked welded structures could be found in [8].

The aforementioned literature showed that HFMI-treatment can be used for fatigue life extension of existing structures even in the presence of small cracks. However, the causatives of fatigue life extension and the mechanisms of improvement need to be furtherly studied. Moreover, the role of mean stresses (e.g. residual stresses) in crack growth retardation has not -to the best of the author's knowledge- been considered before in fatigue life calculation of HFMI-treated cracked transverse attachment. This paper contributes to the comparison of crack-free and cracked details enhanced by HFMI-treatment through fatigue testing. Moreover, this paper is the first to include a fatigue life estimation of cracked transverse attachment repaired by HFMI-treatment, including the residual stress and the existing crack size using fracture mechanics analyses.

2. Experimental program

2.1. Material properties and geometry

Based on the literature review, an experimental program was set up consisting of 31 full penetration butt welded transverse attachment specimens. The specimens were made of carbon mild steel S355 and the filler material for welding was made of core weld C6LF (i.e. metal-cored wire). The chemical compositions and the mechanical proprieties of both are given in Table 1. The properties and the compositions were obtained from the materials' certificates [21,22]. The dimensions of the specimens are shown in Fig. 1.

2.2. Welding and specimen's fabrication

Before welding, the edges of the attachment were machined and chamfered with a nose angle of 30 degrees to reduce the risk of 'lack of fusion'. Metal active gas welding with a Mison18 shielding gas was used. The attachment was then tack-welded to the base plate and a 3 mm gap was left between the two plates. Then, two subsequent welding runs (i.e. root and cap welding) were performed with an approximate throat thickness of 3 mm each. The welding procedures are shown in Fig. 2. The welding parameters for both runs are given in Table 2. Noticeably, no remarkable differences could be found between the parameters of the root and cap welding.

2.3. Fatigue testing

Test frame was set up to test the welded specimens in the ship structural design and analysis laboratory of Hamburg university of technology. An axial testing rig was used to generate pulsating tensile loading. The loads were transferred to the base plate through hydraulic clamps from both sides, see Fig. 3. In addition to the membrane stresses due to axial loads, unintentional bending stresses were present in the weld area because of straightening the specimens by the clamping jaws.

Table 1
The chemical composition and the mechanical proprieties of S355 steel and C6LF filler.

Chemical composition		C	Si	Mn	S	P
S355	%	0.23	0.05	1.6	0.05	0.05
C6LF	%	0.03	0.73	1.51	0.01	0.01
Mechanical properties	Yield strength (MPa)		Ultimate strength (MPa)		Elongation (%)	
S355	355		575		22	
C6LF	459		557		31	

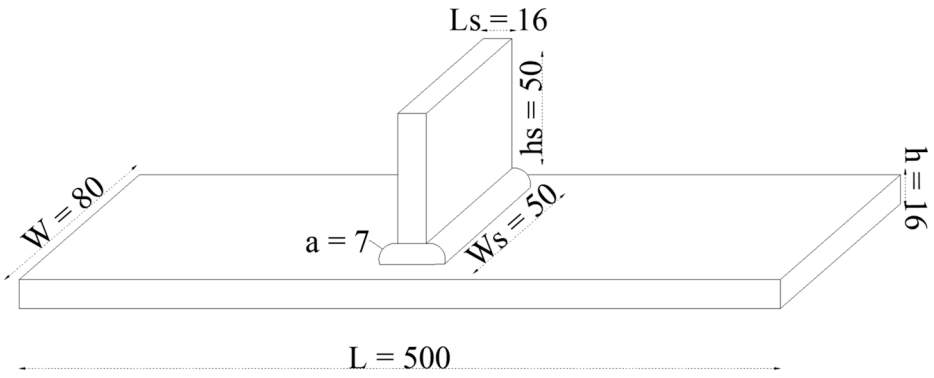

Fig. 1. The specimens geometry (dimensions are given in mm).

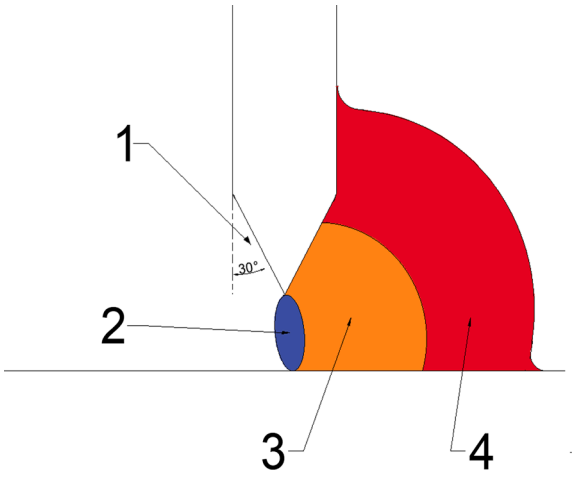

Fig. 2. Welding procedures 1: Machining the stiffener 2: Tack welding 3. Root welding 4. Cap welding.

Table 2
Welding parameters.

Pass	Run	Current (A)	Voltage (V)	Speed (mm/sec)	Heat input (KJ/mm)	Stick-out (-)
1	Root welding	240	28.3	5.8	0.9	15–16
2	Cap welding	235	28.3	5.6	0.95	15–16

The specimens were tested with a stress ratio of 0.29 and a loading frequency of 30 Hz. The positive stress ratio was chosen in order to simulate the real condition in a bridge where the sustained dead load is considered. The specimens were instrumented with several strain gauges at their weld toes for crack detection purposes as illustrated in Fig. 4. The specimens were categorised into five groups as shown in Table 3.

2.4. Auxiliary investigations and measurements

Fatigue testing was supported with several auxiliary investigations; these investigations were essential to get an insight into the local

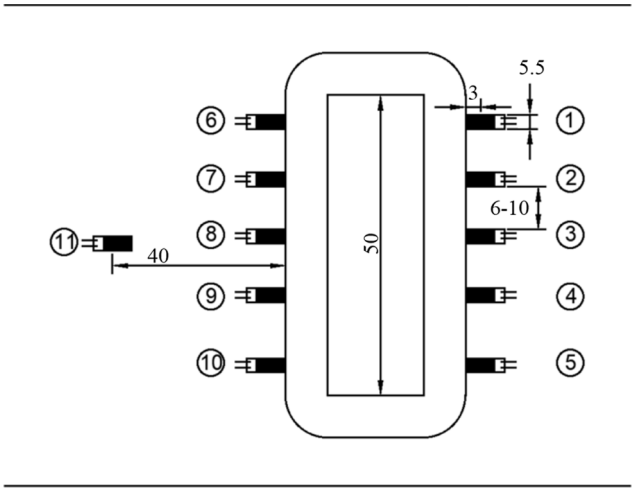

Fig. 4. Strain gauge configuration on test specimen.

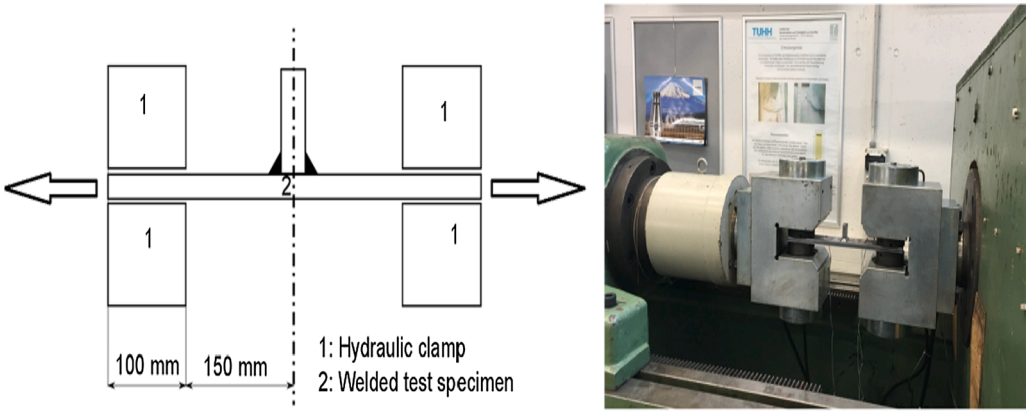

Fig. 3. L: Schematic figure shows the hydraulic clamp. R: Fatigue testing rig.

Table 3
The specimen's series.

Series	Number	Function	SGs	Specimens	Stop criteria
A	12	Investigating the strength of the as-welded specimens	1	1–10,12–13	Failure/Run-out
B	3	Crack detection and calibration	11	14–16	50–80% drop in strain
C	2	Investigating the HFMI effects on existing cracks	5	17–18	50–80% drop in strain
D	8	Investigating the strength of new HFMI specimens	9	21–28	Failure/Run-out
E	6	Investigating the strength of pre-fatigue HFMI specimens	11	29–35	Before HFMI: 25% drop in strain After HFMI: Failure/ Run-out

material and geometrical characteristics before and after HFMI-treatment. These investigations are:

- Crack detection by strains gauges and ultrasonic scanning.
- Topography investigation using a 3D scanner.
- Residual stress measurement by hole drilling method.
- Local Hardness testing by a Vickers hardness tester.
- Microscopic analysis by an optical microscope.
- Angular distortions measurement by a digital calliper.

3. Results

3.1. Fatigue crack inspection and repair

The specimens in series B were used for calibrating crack size against strain drop measured by strain gauges. Fatigue testing was performed on these specimens and continuous strain signals were recorded. Meanwhile, the back wall of the specimens was scanned by an ultrasonic device to track the crack propagation and a dye penetrant was applied periodically to check the crack length. Afterwards, the specimens were cut, and all crack surfaces were examined. Fig. 5 shows the obtained correlation between the maximum recorded strain drop in any of the attached strain gauges and the crack size for different specimens. The figure also shows that a strain drop of 25% of its original value corresponds to a crack size of 0.6–1.2 mm. The obtained scatter in the crack size is traced back to the possibility of crack initiation between two adjacent strain gauges; which implies that the crack will not be sensed by the gauge until it propagates and becomes deeper. On the other hand, if the crack initiates in front of the strain gauge, it will be sensed early, and 25% strain drop will be corresponding to a short crack. It is noteworthy that this percentage is only valid for crack detection in transverse attachment details similar to the one shown in Fig. 1 and instrumented with several strain gauges placed 3 mm off the weld line as shown in Fig. 4.

The specimens in series E were prefatigued until a 25% strain drop was reached. The prefatigue number of cycles varied from specimen to another (as shown in Fig. 6) Because of the difference in crack initiation positions with respect to the closest strain gauge as mentioned above. Moreover, the fatigue lives of different specimens -despite being identical- are expected to be scattered. On the contrary, the specimens in series D were virgin before treatment (i.e. not subjected to any prefatigue loading). Subsequently, the weld toes of the specimens in series D and E were treated by HiFIT indentor. Single indentor tool with a 3 mm diameter was used, the inclination angle of indentor's axis with respect to the base plate surface was fixed to be 60–70 degrees. The groove depth sufficiency was checked using a depth gauge. The treatment intensity for this kind of device is around 180–300 Hz at the weld toe. The device weighs less than 2 kg. More details about the treatment using HiFIT indentors can be found in the international institute of welding's (IIW) recommendation for HFMI-treatment [4].

3.2. Local geometry investigations

Because of the importance of geometry investigation in evaluating the HFMI-treatment efficiency, the local topographies of specimens were scanned by a 3D Winteria scanner before and after HFMI-treatment. Witeria AB visual system is based on a laser line scanner which built up a 3D surface of the bead. The investigated parameters were the weld toe radius and the depth of eventual undercut in as-welded condition or the depth of the groove after HFMI-treatment, see Fig. 7. The probability density functions of the measured parameters are shown in Fig. 8, and the average values are given in Table 4. Noticeably, the toe radius was significantly increased by HFMI-treatment, and the average groove depth was in line with the recommended value by the IIW [4]. Moreover, the consistency of HFMI-treatment can be demonstrated as the coefficient of variation of the toe radius decreased after the treatment as shown in Table 4.

The stress concentration factors were obtained by finite element analyses using the commercial software ABAQUS CAE 2017. A reference toe radius of 1 mm was used for the as-welded specimens, while the obtained average radius after HFMI-treatment + 1 mm was modelled for the HFMI-treated specimens according to the IIW guidelines [23]. 2D 4-nodal shell elements (i.e. CPS4R in Abaqus notations) were used with an element size of 3 mm, the mesh was refined around the weld toe and 0.1 mm local mesh size was adapted. Symmetry boundary conditions were considered in the middle of the attachment and a reference tensile

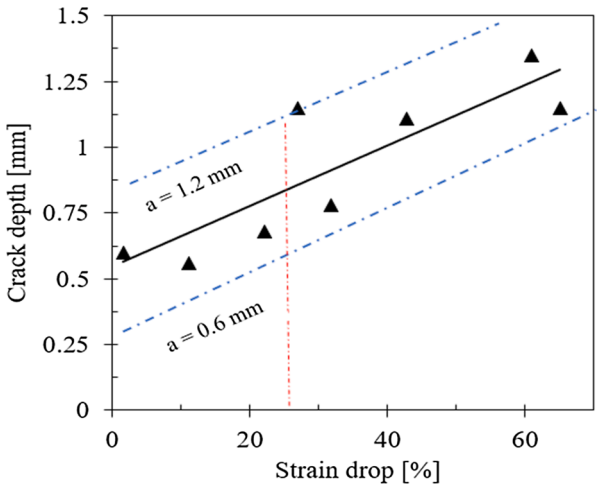

Fig. 5. Crack depth vs strain drop correlation.

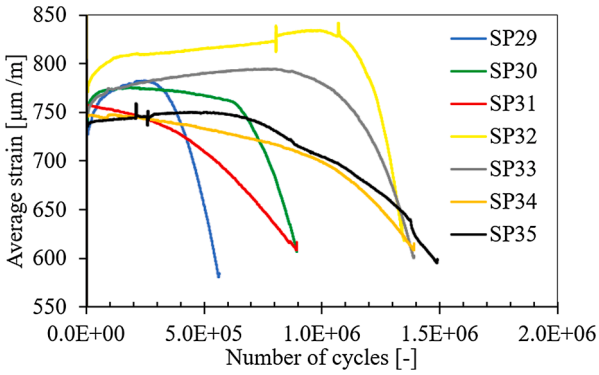

Fig. 6. Examples on strain measurements in series E.

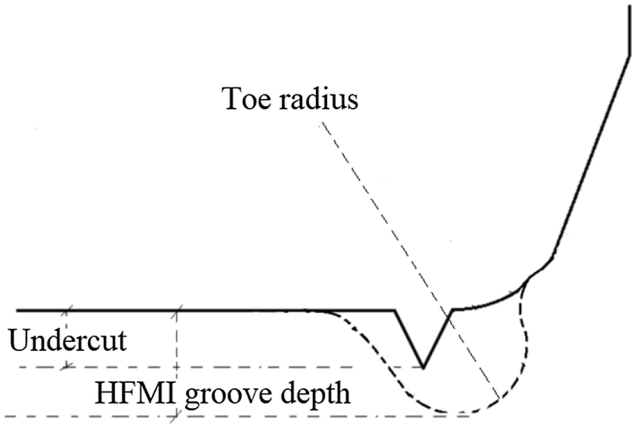

Fig. 7. The investigated parameters in laser weld scanning.

traction of 1 MPa was applied. The stress concentration factors at the weld toe were equal to 2.1 and 1.7 before and after HFMI-treatment respectively. The stress concentration factors in the thickness direction and the model description are shown in Fig. 9.

3.3. Residual stress investigations

The induced compressive residual stress at the weld toe is one of the main beneficial effects of HFMI-treatment as mentioned before. Therefore, the residual stress was investigated by means of hole drilling technique in both as-welded and HFMI states. Several holes were drilled at the weld line in as-welded condition and close to the edge of the HFMI groove as shown in Fig. 10. Table 5 gives the maximum compressive residual stresses and their corresponding depth. The average residual stress distributions are plotted in Fig. 11. Remarkably, compressive residual stresses were dominant at the weld toe even in as-welded conditions. Despite being uncommon, compressive residual stresses could be found at the surface in a few cases summarized in [24]. This might be explained by the expansion of volume due to martensite transformation at the lower temperature [25]. The maximum induced compressive residual stress after HFMI-treatment could be found at around 0.25 mm from the surface of the measured section which coincides with the HFMI groove depth as shown in Table 4 and Fig. 8. Table 5 shows that the HFMI induced compression is 2–3 times larger than stresses in as-welded conditions.

The residual stress distribution could not be directly derived from the measurements for two reasons: the first is related to the accuracy of the measurement which decreases as the measuring depth increases. Besides, only 0.5 mm from the surface were investigated. Therefore, measurements on several details treated by several devices (e.g. ultrasonic impact treatment, needle peening, HiFIT) were collected from the literature. More than 20 research articles containing 33 distributions in the plate thickness direction were analysed to investigate the depth of the induced compression (Yc), and the maximum induced compressive residual stress [5,6,19,26–43]. The results of the literature review are shown in Fig. 12.

The collected literature includes measurement on several detail types (e.g. transverse and longitudinal attachment) with different base plate thicknesses varying from 5 to 60 mm, the studied yield strength in the literature varies from 235 to 960 MPa. Fig. 12 shows that the obtained depth of induced compression varies between 0.8 mm and 3.7 mm depending on many factors such as depth of indentation and material type [5,19]. Besides, the figure also shows that the maximum compressive residual stress is close to the yield strength which is in line with the measured values given in Table 5.

The distribution of residual stress in the as-welded condition was constructed in accordance with the British standard recommendation for metallic structures [44]. The surface values were obtained from the residual stress measurements given in Table 5 and the depth of compression was assumed to be 5% of the plate thickness [24]. The maximum and minimum measured compressive residual stresses given in Table 5 was combined with the most probable depth of compression in the literature (which is between 1.5 and 2 mm as shown in Fig. 12) to construct the distributions of residual stresses after HFMI-treatment, see Fig. 13.

3.4. Hardness testing

Vickers microhardness measurement with a test load of 3 Kg was used to determine the hardness distribution in the weld toe vicinity. Rectangular grids were created, and indents were spaced 0.5 mm apart vertically and horizontally. Additional 5 measurement points were added along the weld line and parallel to the weld edges. The hardness contour in as-welded and HFMI conditions are shown in Fig. 14, and the distributions below the toe are depicted in Fig. 15. A remarkable

Table 4
The local geometrical parameters for the specimens in as-welded and after HFMI-treatment.

Series	AW		HFMI	
	Toe radius	Undercut	Toe radius	Groove depth
Mean	0.67 mm	0.004 mm	1.2 mm	0.26 mm
Standard deviation	0.31 mm	0.03 mm	0.29 mm	0.13 mm
Variation coefficient	0.46	8.74	0.24	0.51
Population	20,660	20,660	1331	1653

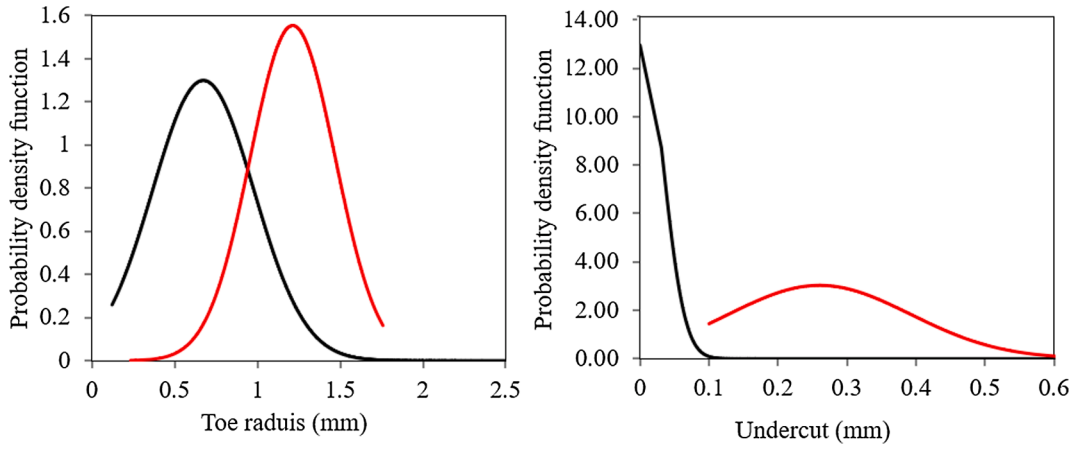

Fig. 8. The probability density functions on the weld toe radius and undercut (HFMI groove).

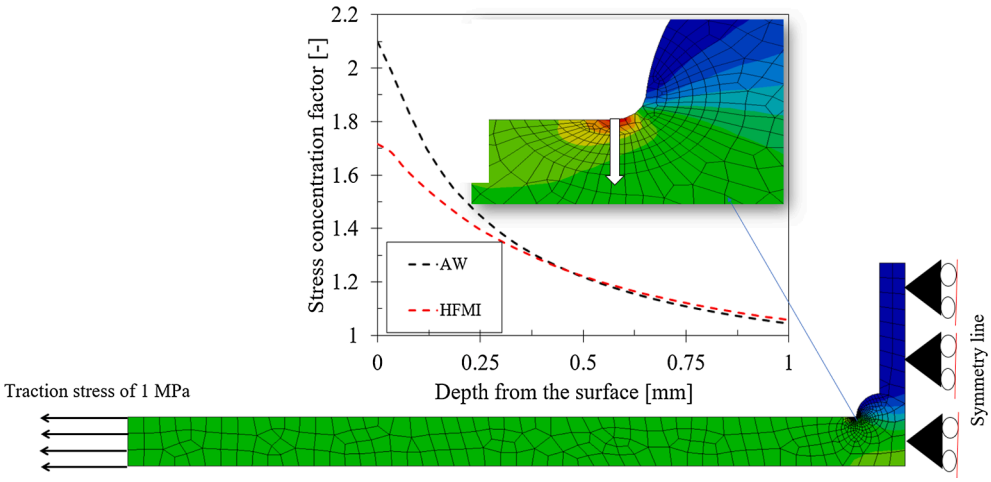

Fig. 9. Model for evaluating the stress concentration factors of the as-welded and HFMI-treated specimens.

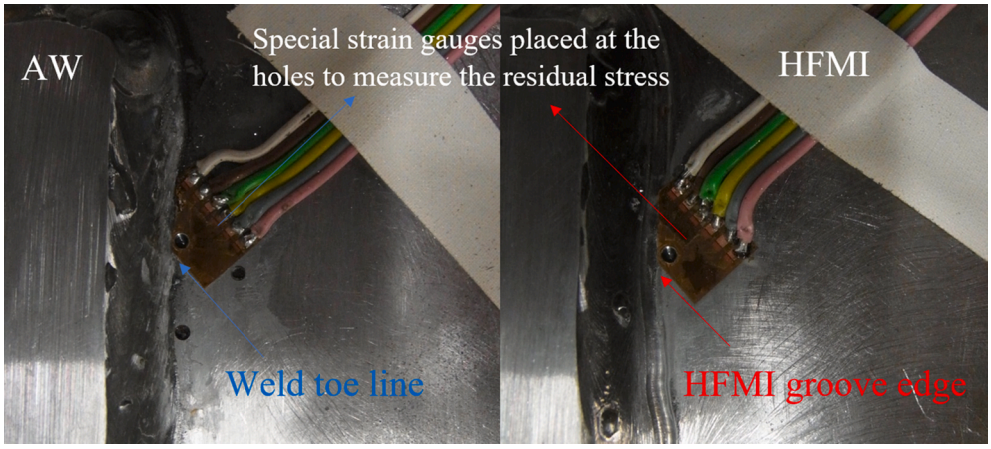

Fig. 10. Hole drilling on as-welded and HFMI-treated specimens.

Table 5
Residual stress measurement results.

Status		Maximum σ_{RS} (MPa)	Depth of maximum σ_{RS} (mm)
Average	AW	−185	0.1
	HFMI	−375	0.24
Maximum	AW	−265	0.1
	HFMI	−430	0.28
Minimum	AW	−104	0.1
	HFMI	−330	0.18

increase in the hardness at the weld toe from 180 HV3 in the as-welded state to 220 HV3 after HFMI-treatment was observed. However, this HFMI effect became faint at 2 mm from the surface.

3.5. Distortion and clamping stress investigations

The angular distortion (α) of several as-welded and HFMI-treated specimens was measured and the average values are plotted in Fig. 16. Several measurement points were considered along the specimens in two parallel lines (A and B). Remarkably, the angular distortions decreased after HFMI-treatment. Besides, the treatment also reduced the twist of the specimens which caused the 2 curves corresponding to the HFMI-specimen in the figure to overlap each other. Different angular distortions induced different bending stresses when the specimens got straightened. Therefore, an additional source of fatigue life scattering was introduced.

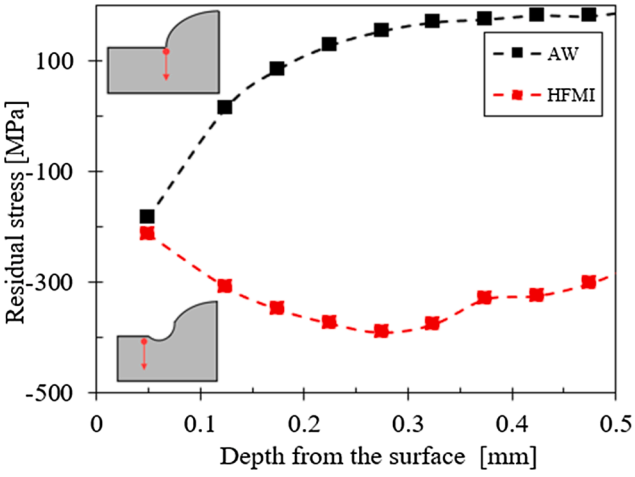

Fig. 11. The In-depth residual stress distribution of the as-welded and HFMI-treated specimens.

Unintentional bending stresses were introduced to the specimens due to clamping as mentioned in Section 3. The nominal clamping stresses were obtained from the attached strain gauges at a distance of 40 mm off the welds (i.e. strain gauge 11 in Fig. 4). However, the notch stress at the weld toe could not be obtained directly. Therefore, a 2D linear elastic

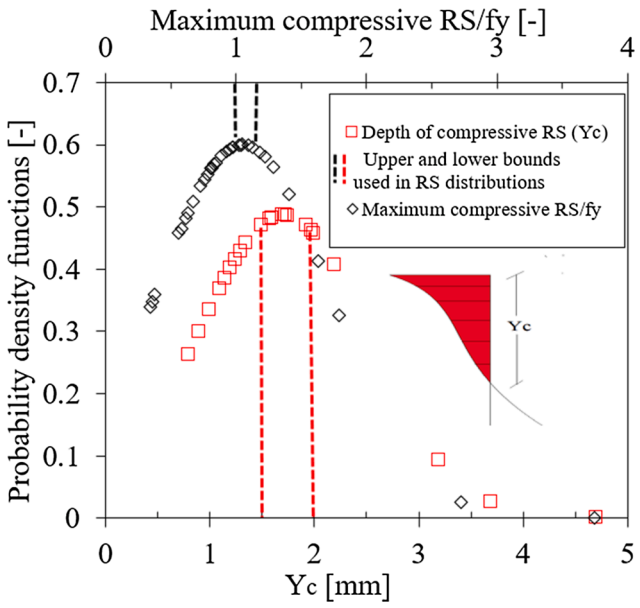

Fig. 12. The probability density functions of the HFMI-induced compression and its depth.

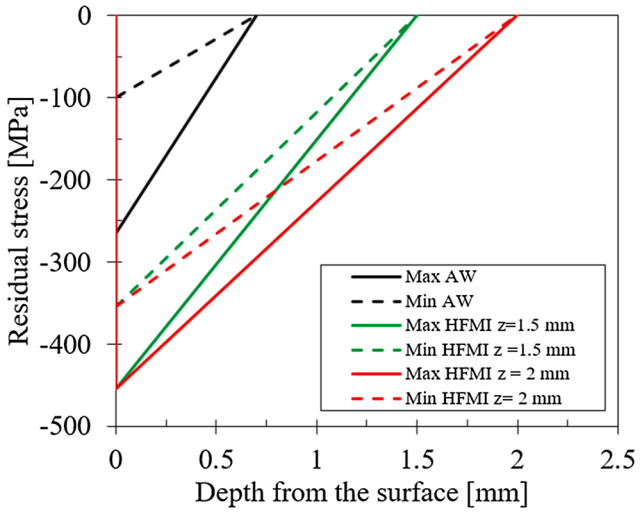

Fig. 13. Suggested residual stress distributions for as-welded and HFMI-treated specimens.

finite element analysis was conducted using the commercial software ABAQUS/CAE 2017. In order to avoid stress singularity at the weld toe, a fictitious radius of 1 mm was assumed in the model analogously to the effective notch method. Plane stress shell elements (CP4SR in Abaqus notation) were used to create the mesh. The local mesh size was selected following the IIW recommendations for the effective notch approach [45], and convergence study showed that a local mesh size of 0.025 mm around the weld toe led to converged results. A global mesh size of 2 mm was considered for the rest of the model.

Several models were created with different geometries based on the measured distortions of different specimens. Poisson's ratio and elasticity modulus were selected to be 0.3 and 210 GPa, respectively. The clamping jaws of the test rig were modelled as undeformable objects approaching each other in a deformation control manner (Uy was prescribed). The displacement of the jaws in the transverse direction was restricted (Ux = 0). Besides, hard normal contact was defined between the master surface (i.e. the clamping jaws) and the slave surface (i.e. the specimen's surface); the model is illustrated in Fig. 17. The results were extracted when the specimens got fully straightened (i.e. the surface of the specimen became parallel to surfaces of the clamping jaws). A good match between the clamping stresses evaluated experimentally (the red curve in Fig. 18) and the FE-results (the black curve in the same figure). Therefore, the model was validated, and notch stresses were extracted and given by the blue curve in the figure. The obtained clamping stresses, the distortion angles (∅) and the corresponding uplift of the specimen ends are given in Table 6. Further, the clamping stress distributions below the weld toe are extracted in Fig. 19.

The secondary bending stresses are included in the IIW recommendations by magnifying the membrane stress range by a stress magnification factor [45]. This factor is dependent on the geometry of the base plate and the uplift in the specimen given in Table 6. It is also dependent on the applied stress range. For the studied geometry, the recommended additional stresses due to average clamping values given in the table were found to be equal to 42, 48 and 52 MPa in as-welded conditions and 34, 38 and 42 MPa after HFMI-treatment when the applied stress ranges are 150, 180 and 210 respectively. These values were less than the experimentally obtained average clamping stresses given by the red curve shown in Fig. 18.

3.6. Microscopy

After prefatigue loading, the specimens in series C were cut in a direction perpendicular to the weld line to perform a metallographic investigation. Then, the surfaces were ground by rubbing against wet sandpapers and artificial diamond paste. Finally, they were processed by etching with 2% V/v Nital solution. Two examples of the processed surfaces are shown in Fig. 20. For the studied crack size (0.6–1.2 mm), a remarkable reduction in the crack width and a change in crack orientation with an angle of 5–15 degrees with respect to the attachment direction were observed. Besides, a previous study presented a 2D elastoplastic finite element simulation of the HFMI-treatment process of the cracked welded detail. Friction was assumed between the crack surfaces and between the indentor and the specimen's surface. The indentor was modelled as a rigid undeformed body and the displacement was prescribed so that the indentation depth reached specific values. The study showed that HFMI-indentor induces compressive plastic strain at the crack tip. However, the area of the compressive plastic strain zone decreases as the crack size increases [19], see Fig. 21.

3.7. Fatigue test results

The as-welded and HFMI-treated specimens were tested under the same stress ratio and loading frequency as mentioned in Section 3. Fatigue test results are given in Table 7 and fatigue strength curves are shown in Fig. 22. The specimens in series A, D and E were depicted in the figure as ''AW'', ''New HFMI'' and ''Prefatigued HFMI'' respectively. The characteristic fatigue strength curves for both as-welded and HFMI-treated transverse attachments according to the IIW recommendations [4,45] are denoted in the figure by the solid black and red curves respectively. In series D (New HFMI) and series E (Prefatigue HFMI), many specimens ran-out after 10 million cycles when tested at a stress range of 150 MPa without observing any local strain drop. Therefore, the applied stress ranges were increased to 180 or 210 MPa. Subsequently, all the HFMI-treated specimens failed at the weld toe.

After excluding the run-out results, The obtained characteristic fatigue strengths (i.e. FAT values) were found to be 125, 180 and 165 MPa for AW, prefatigued HFMI and new HFMI series respectively. The FAT values were calculated using the ''prediction interval method'' with a free slope [46]. The calculated FAT values represent the fatigue strength for 95% probability of survival (i.e. low probability of failure). The as-welded specimens were 4 classes stronger than the assigned fatigue strength in EN1993-1–9 for transverse attachments [47]. Remarkably, the prefatigued specimens which contained cracks have stronger FAT value than the ones corresponding to the virgin ones by around 10%.

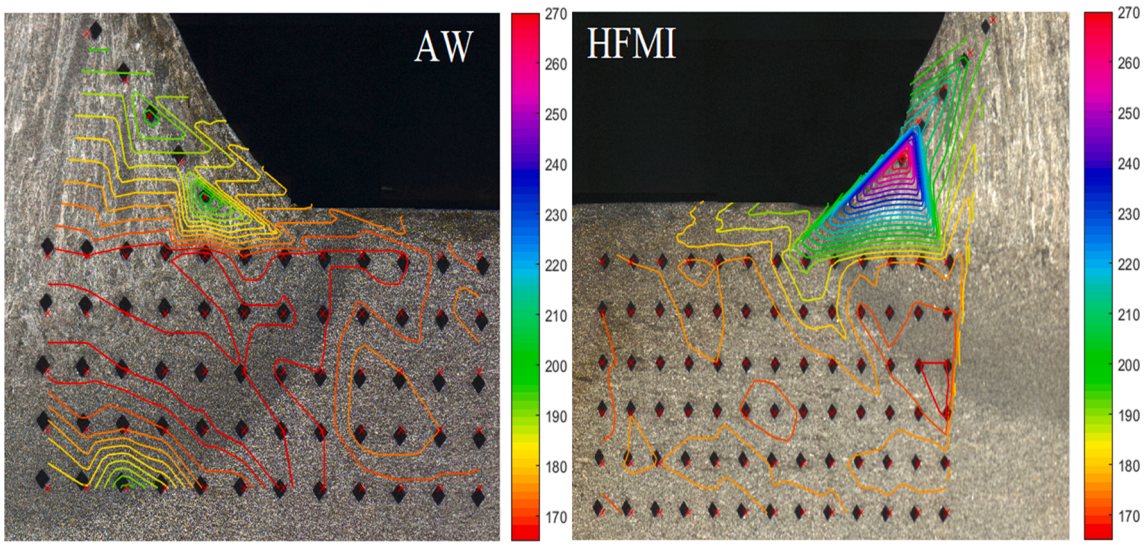

Fig. 14. Hardness measurement (HV3) distribution for as-welded and HFMI-treated specimens respectively.

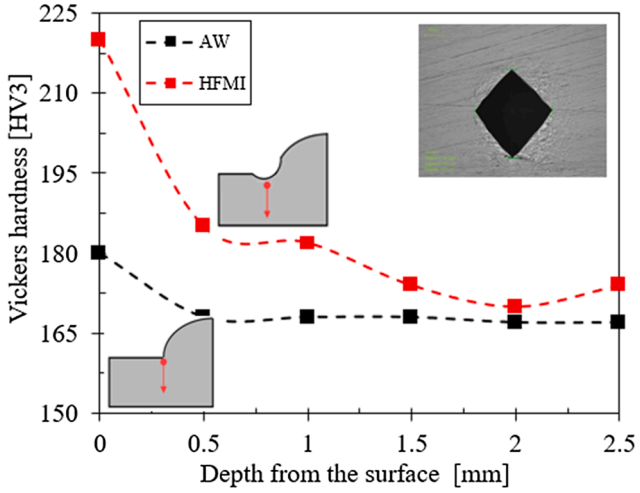

Fig. 15. Vickers hardness distributions below the weld toe of the as-welded and HFMI-treated specimens.

Nevertheless, both mentioned series were stronger than the base metal which has a FAT value of 160 MPa [47].

4. Discussion

The long obtained fatigue lives of the as-welded specimens were the result of the presence of compressive residual stress at the weld toe as shown in Table 5 and Fig. 22. However, this effect was reduced by the tensile clamping stresses as given in Table 6. On the other hand, HFMI-treatment caused a further increase in fatigue life because of several reasons. The most prominent one was the high introduced compressive residual stress at the weld toe. The reduction in the stress concentration because of the increase in toe radius after HFMI-treatment was another factor. In addition, the increase in hardness due to local cold working below the HFMI-groove caused an increase in the local ultimate strength from 575 to 700 MPa. Moreover, the additional mean stresses due to clamping were reduced after HFMI-treatment because of the reduced distortions as shown in Fig. 16.

Since only seven prefatigued HFMI specimens were tested in this paper, additional fatigue test results were collected from the literature [7,9,10,20] to validate the use of HFMI as an efficient fatigue life extension method in transverse attachments. The collected data was obtained on specimens with crack size less than 4 mm. No distinction was made in the evaluation with reference to mean stress, stress ratio or

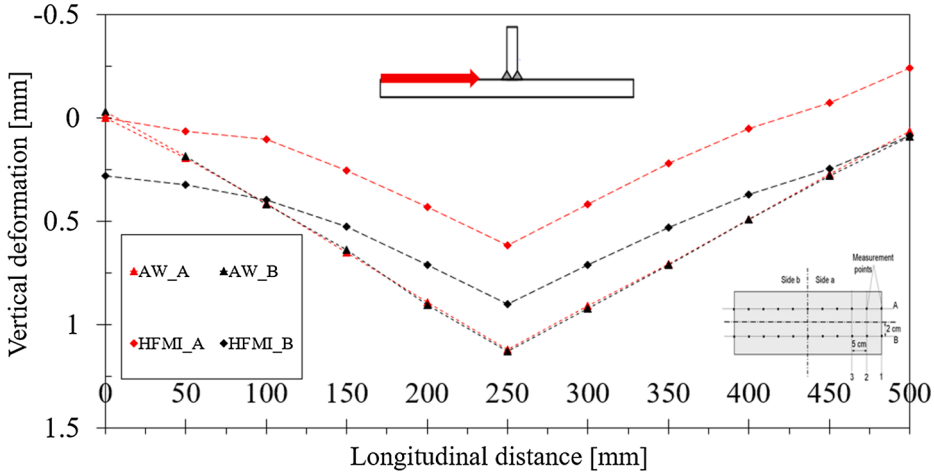

Fig. 16. The average angular distortions of the specimens in as-welded and HFMI-treated states.

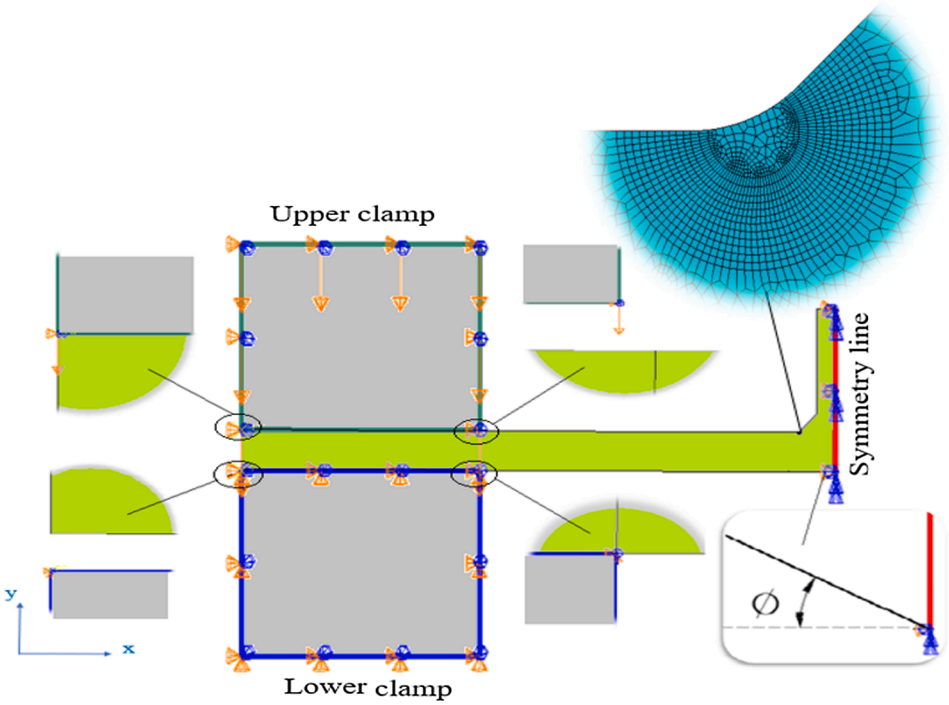

Fig. 17. 2D numerical model for the clamping process of specimens with a specified angular distortion (∅).

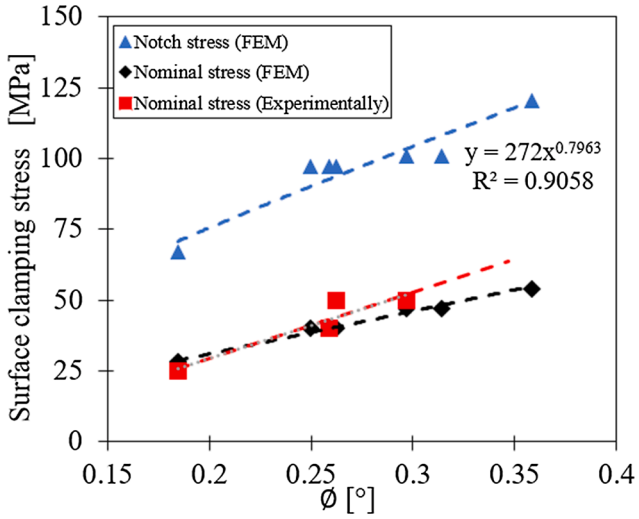

Fig. 18. The correlation between the angular distortion and nominal, local clamping stresses.

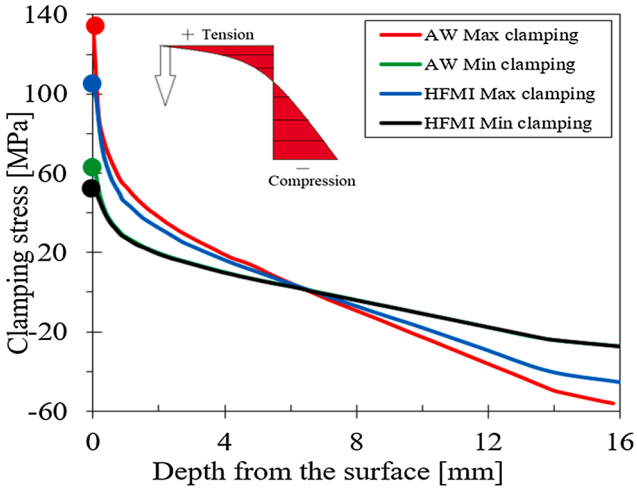

Fig. 19. Maximum and minimum clamping stress distributions.

Table 6
Average clamping stress before and after treatment.

Status		Angle (°)	Uplift (mm)	Notch stress (MPa)
Average	AW	0.29	1.25	100
	HFMI	0.23	0.99	83
Maximum	AW	0.41	1.79	134
	HFMI	0.29	1.25	98
Minimum	AW	0.17	0.72	65
	HFMI	0.14	0.59	55

plate thickness. In addition, several test results for virgin HFMI-treated specimens (i.e. crack-free specimens) of the same detail were collected also from the literature [6,10,48–50]. The results are shown in Fig. 23. None of the green and red circles in the figure (i.e. prefatigued HFMI) is lying under the characteristic curve of new HFMI-treated detail. In some cases, prefatigued specimens showed higher fatigue strength than the crack-free specimens (i.e. black and blue data points). This indicates the efficiency of HFMI-treatment in fatigue life extension even with the presence of cracks up to 4 mm. Thereby, fatigue life extension of transverse attachment details containing crack (0.6–1.2 mm) using HFMI-treatment was proven by both the literature study and the fatigue testing in this paper.

In order to get an insight into the effect of residual stresses, clamping stresses and existing crack sizes, linear elastic fracture mechanics analyses were performed. Stress intensity factors were estimated to predict the fatigue life of the studied transverse attachment in as-welded and HFMI conditions. The stress intensity factors were calculated by integrating the product of the weight function m(x, a) (obtained from [51]) times the stress profile along the prospective crack path for the uncracked specimens σ_x as shown in equation (1). σ_x can accommodate

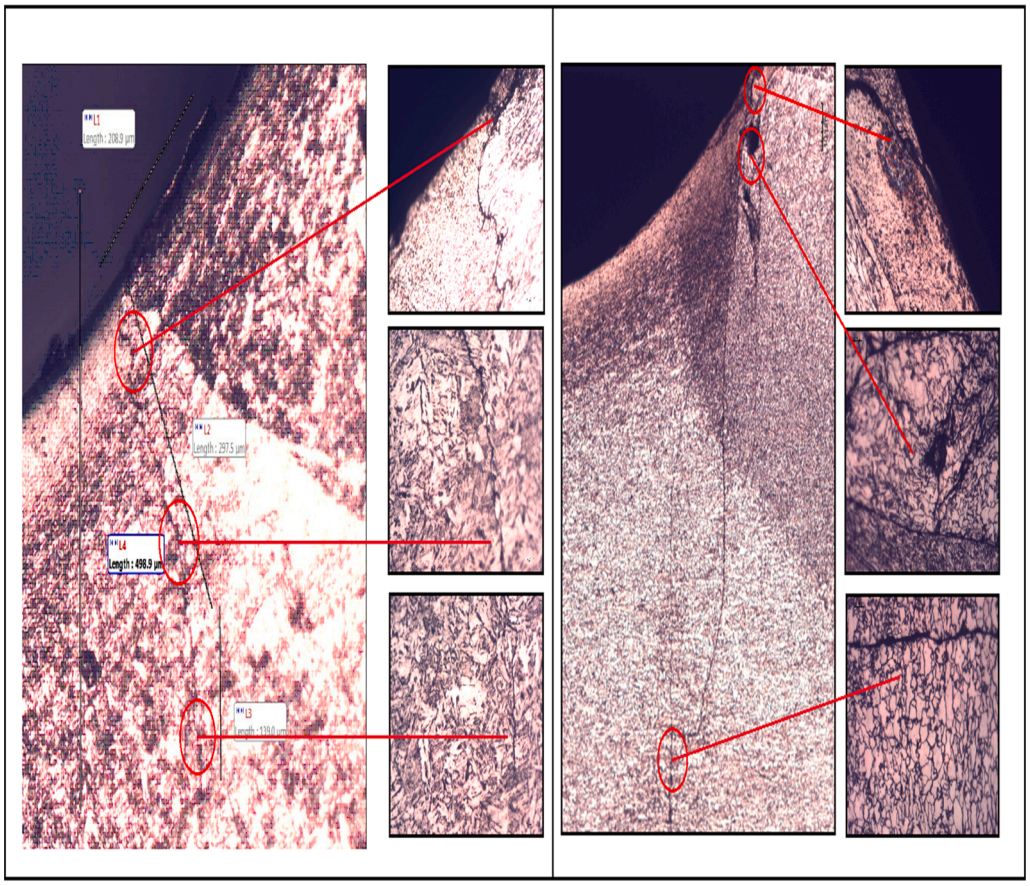

Fig. 20. Observations of the crack shapes after HFMI-treatment for different specimens.

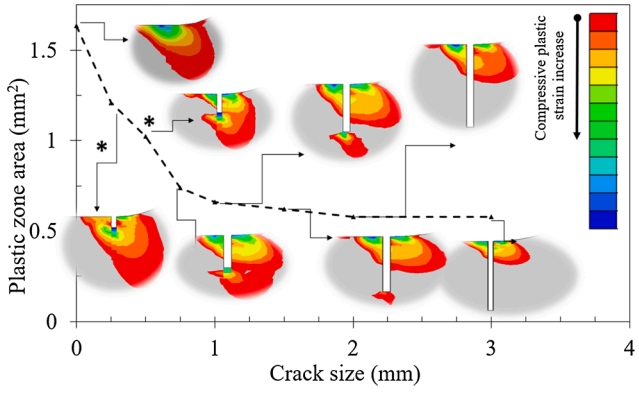

Fig. 21. Compressive plastic zone size for different crack sizes [19].

any stress field such as the stress range Δσ, the maximum stress σ_{max}, the minimum stress σ_{min}, the residual stress σ_{RS} and the clamping stress σ_{cs} [6,8,51–53]. To increase the precision of the analyses, the stress concentration factors shown in Fig. 9 were used to estimate the local stress fields. In addition, residual stress distributions shown in Fig. 13 were incorporated in the definition of the effective stress ratio R_{eff} given by equation (2). The IIW recommendations for consideration of clamping stresses gave unconservative results as mentioned in Section 3.5. Therefore, the distributions shown in Fig. 19 (which were obtained from finite element analyses and compared to experimental results) were incorporated instead in the definition of R_{eff}. Subsequently, the crack propagation increment da was calculated by equation (3) using dN = 5000 cycles. These three equations are obtained from [8] with an adjustment to incorporate the clamping stresses in the analyses.

$$K = \int_0^a m(x,a).\sigma(x).dx \tag{1}$$

$$R_{eff} = \frac{K_{min} + K_{RS} + K_{CS}}{K_{max} + K_{RS} + K_{CS}} \tag{2}$$

$$da = \begin{cases} \left(C.\frac{(K_{max} - K_{\min})^m}{(1.5 - R_{eff})^m}.dN, if\, K_{max} - K\_min > K_{th} \right. \\ \left. 0, Otherwise \right. \end{cases} \tag{3}$$

Where C and m are characteristic material parameters and their values were taken as $1.65.10^{-11}$ m/(cycle.(MPa.$m^{0.5}$)^3) and 3 respectively, and the threshold stress intensity K_{th} was selected to be 2 MPa. $m^{0.5}$, in accordance with [45]. The characteristic values of C, m and K_{th} were used because it is recommended to use them if the assessment is to be conducted for welded joints [44]. Two initial crack sizes in as-welded conditions were studied: 0.15 and 0.5 mm. The former was selected according to the IIW recommendations while the latter is the maximum permissible undercut height for transverse attachment according to the British standard for welding [54]. On the contrary, the initial crack size for prefatigued HFMI-treated specimens was selected to be 0.6 and 1.2 mm in accordance with the inspection results given in Section 3.1.

The results of the analyses for as-welded specimens are shown in Fig. 24. Several curves were generated with different combinations of the initial crack size a_i, residual and clamping stresses (The summation of both these stresses at the weld toe is depicted in the legends by RS + CS). Twenty-two data points from the experiments were also plotted on the same figure; these points include the full fracture of the as-welded specimens (a = 16 mm) and the prefatigue loading stage of specimens in series E. Only 4 data points were off the estimation limits with a maximum error of 10%. The error is explained by the uncertainty in the

Table 7
Fatigue tests results.

Test	Specimen	Δσ (MPa)	N (cycles)	Abort criterion	Test	Specimen	Δσ (MPa)	N (cycles)	Abort criterion
As-welded (series A)									
A1a	1	119	1.00E7	Run-out	A4	4	145	1.08E6	Failure
A1b	1	143	2.15E6	Run-out	A5	5	175	7.57E5	Failure
A2a	2	114	7.85E6	Run-out	A6	6	170	6.85E5	Failure
A2b	2	125	1.04E7	Run-out	A7	7	165	8.59E6	Failure
A2c	2	140	8.00E6	Run-out	A8	8	160	9.87E6	Failure
A2d	2	132	2.75E6	Run-out	A9	9	150	1.13E6	Failure
A2e	2	145	8.84E5	Failure	A10	10	150	1.60E6	Failure
A3a	3	132	2.53E6	Run-out	A12	12	150	3.25E6	Failure
A3b	3	139	3.10E6	Failure	A13	13	150	2.42E6	Failure
Virgin HFMI-treated (series D)									
D21a	21	180	1.00E7	Failure	D26	26	150	4.41E6	Failure
D21b	21	180	9.12E5	Run-out	D27a	27	150	1.00E7	Run-out
D22	2.2	150	4.32E6	Failure	D27b	27	180	1.38E6	Failure
D23	23	150	5.82E6	Failure	D28a	28	150	1.00E7	Run-out
D24	24	150	2.19E6	Failure	D28b	28	180	1.00E7	Run-out
D25a	25	150	1.00E7	Run-out	D28c	28	210	1.03E6	Failure
D25b	25	180	3.88E6	Failure					
Prefatigue stage (series E)									
E29P	29	150	5.64E5	25% strain drop	E33P	33	150	1.38E6	25% strain drop
E30P	30	150	8.93E5	25% strain drop	E34P	34	150	1.42E6	25% strain drop
E31P	31	150	8.94E5	25% strain drop	E35P	35	150	1.49E6	25% strain drop
E32P	32	150	1.34E6	25% strain drop					
Prefatigued HFMI-treated (series E)									
E29a	29	150	1.00E7	Run-out	E32c	32	180	2.14E6	Failure
E29a	29	180	1.89E6	Failure	E33a	33	150	1.00E7	Run-out
E30a	30	150	1.00E7	Run-out	E33b	33	210	8.25E5	Failure
E30a	30	180	2.76E6	Failure	E34a	34	150	1.007	Run-out
E31a	31	150	1.00E7	Run-out	E34b	34	150	2.95E6	Failure
E32a	32	150	1.00E7	Run-out	E35a	35	150	1.00E7	Run-out
E32a	32	150	1000E7	Run-out	E35b	35	210	3.78E5	Failure

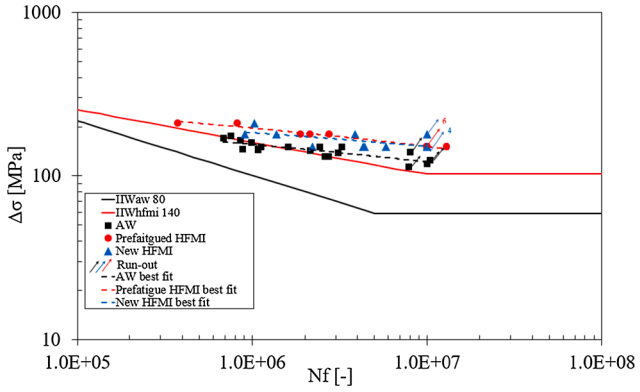

Fig. 22. The fatigue curves of the as-welded and HFMI-treated specimens.

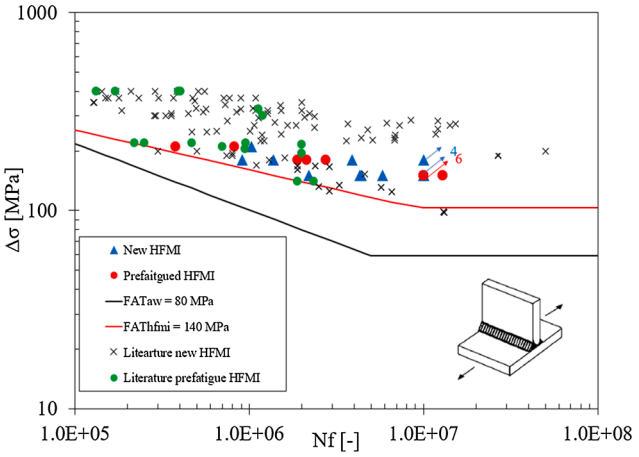

Fig. 23. Fatigue test results of HFMI-treated transverse attachment.

initial crack size which can be smaller than the assumed value of 0.15 mm [8]. Besides, the initial crack size effect was found to be more pronounced for higher residual stresses, see the red and blue curves in the figure. This is explained by the shallowness of the compressive stress field in as-welded conditions, see Fig. 13.

Figs. 25, 26 and 27 depict the analyses results of the prefatigued HFMI-treated detail under different stress ranges. Incorporating K_{th} enabled the analyses to predict the 6 run-outs after 10 million cycles as given in Table 7. Also, 5 out of 6 specimen's fatigue lives could be predicted by the generated curves. Moreover, producing beach marks on the fracture surface of specimen '34' after each half million cycles enabled obtaining additional 4 points in Fig. 25 and found to be corresponding well with the black curve. Despite being cracked, the fatigue lives of the HFMI-treated specimens became longer in comparison to the as-welded ones because of the larger residual stresses and the smaller distortions. Nonetheless, the fatigue lives became shorter under the nominal stress of 210 MPa because the external loading effect overcame the beneficial effects of HFMI-treatment.

The analyses gave an insight into the sources of test results scattering which is attributed to the differences in the introduced compressive residual stress, clamping stress and initial crack size in each specimen. Moreover, the analyses pinpointed the importance of the compressive residual stresses in crack growth retardation and thereby fatigue life extension of existing structures. It should be stated that the model did not consider the residual stress relaxation due to cyclic loading. Besides, simplified residual stress distributions were used which might not be representatives for the real status of the specimens.

5. Summary and conclusions

Within the current study, full penetration butt welded transverse attachment specimens made of S355 structural steel were fatigue tested in three states: As-welded, virgin HFMI-treated and prefatigued HFMI-

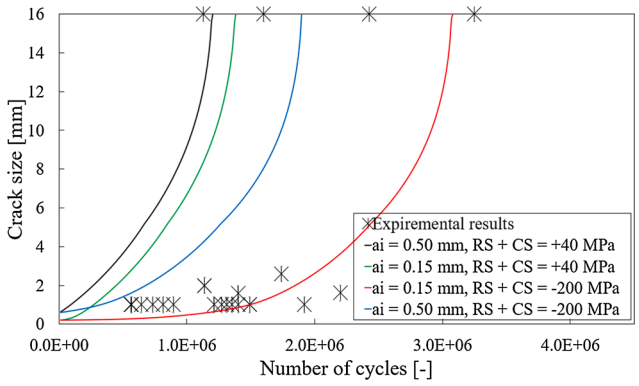

Fig. 24. Crack propagation curves for as-welded specimens under $\Delta\sigma$ = 150 MPa.

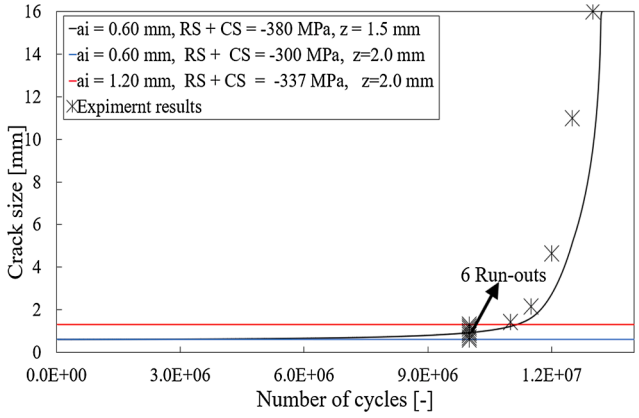

Fig. 25. Crack propagation curves for prefatigued HFMI-treated specimens under $\Delta\sigma$ = 150 MPa.

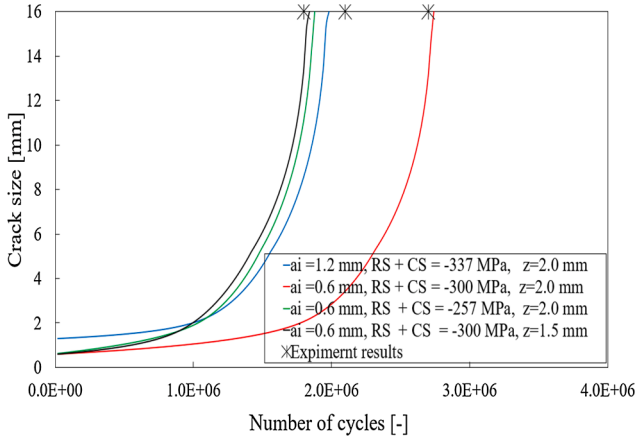

Fig. 26. Crack propagation curves for prefatigued HFMI-treated specimens under $\Delta\sigma$ = 180 MPa.

treated conditions. In addition, crack growth calculations were employed to predict the fatigue lives under different conditions. The results permitted the following conclusions to be made:

- The fatigue strength of the specimens in as-welded conditions was found to be 125 MPa, which is larger than the assigned value for this detail given by the IIW recommendations. This might be traced back to the compressive residual stress at the weld toe in as-welded conditions.

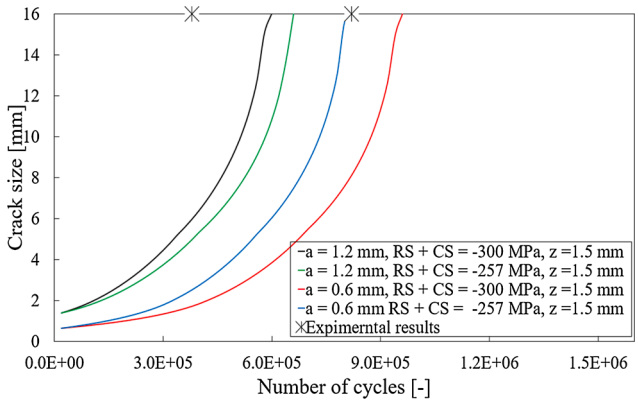

Fig. 27. Crack propagation curves for prefatigued HFMI-treated specimens under $\Delta\sigma$ = 210 MPa.

- HFMI-treatment was found to be an effective method in extending fatigue life even in the presence of cracks in transverse welded details. Fatigue testing has shown that all specimens containing 0.6–1.2 mm deep crack ran-out after 10 million cycles of loading when tested at stress range $\Delta\sigma$ = 150 MPa.
- The fatigue strength after HFMI-treatment was found to be 165 MPa for the new specimens, and 180 MPa for the prefatigued specimens. Both these values are larger than the fatigue strength of the base metal according to the IIW recommendations.
- A literature study was conducted on the use of HFMI-treatment on prefatigued transverse attachment details containing cracks shallower than 4 mm. All the collected fatigue test results showed longer fatigue lives than the characteristic life of the new detail according to the IIW recommendations.
- HFMI-treatment effects on the weld toe vicinity were investigated. The treatment caused weld toe radius and local hardness increase, and angular distortion decrease. Moreover, the treatment changed the crack orientation and induced compressive residual stresses at the weld toe. All these changes demonstrated the physics behind fatigue life improvement of existing structures by HFMI-treatment.
- HFMI-treatment caused a substantial change in the local weld topography where the average toe radius increased from 0.67 mm to 1.2 mm. This caused a reduction in the stress concentration factor at the weld toe from 2.1 to 1.7. Moreover, the local ultimate strength increased from 575 MPa to 700 MPa. However, the effect of the steel hardening became faint at 2 mm from the surface.
- A literature study was conducted on the HFMI-induced residual stress, it was found that the maximum compressive residual stress exceeds the material's yield limit. Moreover, the depth of the induced compression reaches 1.5–2.0 mm in most cases.
- Fracture mechanics analyses were conducted and the effect of mean stress (including residual and clamping stresses) was incorporated to predict fatigue lives. Several crack propagation curves were generated, and the experimental results were in most of the cases in line with the predictions. The main reasons behind the analyses results scattering were the residual stress distributions and the existing crack sizes.

CRediT authorship contribution statement

Hassan Al-Karawi: Conceptualization, Methodology, Investigation, Data curation, Formal analysis, Validation, Software, Visualization, Writing - original draft. **Rüdiger U. Franz von Bock und Polach:** Supervision, Writing - review & editing, Resources, Investigation. **Mohammad Al-Emrani:** Supervision, Writing - review & editing, Resources, Project administration, Funding acquisition.

Declaration of Competing Interest

The authors declare that they have no known competing financial interests or personal relationships that could have appeared to influence the work reported in this paper.

Acknowledgment

The work presented in this paper has been conducted within the research project 'LifeExt' with funding from the Swedish Transport Administration (Trafikverket) and the Swedish Innovation Agency (Vinnova).

Appendix A. Supplementary material

Supplementary data to this article can be found online at https://doi.org/10.1016/j.engstruct.2021.112234.

References

[1] Shams-Hakimi P. Performance of high-frequency mechanical impact treatment for bridge application [Licentiate dissertation]. Department of Architecture and Civil Engineering, Chalmers University of Technology; 2017.
[2] Houjou K, Takahashi K, Ando K, Abe H. Effect of peening on the fatigue limit of welded structural steel with surface crack, and rendering the crack harmless. Int J Struct Integr 2014;5(4):279–89.
[3] Al-Karawi H, Al-Emrani M. The efficiency of HFMI treatment and TIG remelting for extending the fatigue life of existing welded structures. Steel construction 2021. https://doi.org/10.1002/stco.202000053.
[4] Marquis GB, Barsoum Z. IIW Recommendations on High Frequency Mechanical Impact (HFMI) treatment for improving the fatigue strength of welded joints. In: IIW recommendations for the HFMI Treatment. Singapore: Springer; 2016. p. 1–34.
[5] Leitner M, Khurshid M, Barsoum Z. Stability of high frequency mechanical impact (HFMI) post-treatment induced residual stress states under cyclic loading of welded steel joints. Eng Struct 2017;143:589–602.
[6] Shams-Hakimi P, Zamiri F, Al-Emrani M, Barsoum Z. Experimental study of transverse attachment joints with 40 and 60 mm thick main plates, improved by high-frequency mechanical impact treatment (HFMI). Eng Struct 2018;155:251–66.
[7] Branco CM, Infante V, Baptista R. Fatigue behaviour of welded joints with cracks, repaired by hammer peening. Fatigue Fract Eng Mater Struct 2004;27(9):785–98.
[8] Leitner M, Barsoum Z, Schäfers F. Crack propagation analysis and rehabilitation by HFMI of pre-fatigued welded structures. Weld World 2016;60(3):581–92.
[9] Günther HP, Kuhlmann U, Dürr A. Rehabilitation of welded joints by ultrasonic impact treatment (UIT). In: IABSE Symposium Report, vol. 90, no. 4. International Association for Bridge and Structural Engineering; 2005. p. 71–7.
[10] Kudryavtsev Y, Kleiman J, Lugovskoy A, Lobanov L, Knysh V, Voitenko O, et al. Rehabilitation and repair of welded elements and structures by ultrasonic peening. Weld World 2007;51(7-8):47–53.
[11] Zhang H, Wang D, Xia L, Lei Z, Li Y. Effects of ultrasonic impact treatment on pre-fatigue loaded high-strength steel welded joints. Int J Fatigue 2015;80:278–87.
[12] Maddox SJ, Doré MJ, Smith SD. A case study of the use of ultrasonic peening for upgrading a welded steel structure. Weld World 2011;55(9-10):56–67.
[13] Fisher JW, Pense AW, Slockbower RE, Hausammann H. Retrofitting fatigue damaged bridges. Transportation Research Record (664); 1978.
[14] Fisher JW, Sullivan MD, Pense AW. Improving fatigue strength and repairing fatigue damage; 1974.
[15] Fueki R, Takahashi K. Prediction of fatigue limit improvement in needle peened welded joints containing crack-like defects. Int J Struct Integr. 2018;9(1):50–64.
[16] Fueki R, Takahashi K, Houjou K. Fatigue limit prediction and estimation for the crack size rendered harmless by peening for welded joint containing a surface crack. Mater Sci Appl 2015;06(06):500–10.
[17] YuanZhou Z, Ji B, Fu Z, Ge H. Local stress variation in welded joints by ICR treatment. J Constr Steel Res 2016;120:45–51.
[18] YuanZhou Z, Ji B, Sun T, Ye Z. Numerical model of plastic deformation on cracked surface under repeated pneumatic impact. Adv Mater Sci Eng 2018;2018:1–9.
[19] Al-Karawi H, Hedegård J, Al-Emrani M. Crack behavior after high frequency mechanical impact in welded S355 structural steel. The tenth International Conference on Bridge Maintenance, Safety and Management (IABMAS), 11–18 April 2021, Japan. CRC Press -Taylor & Francis Group; 2021. p. 3113–9.
[20] Infante V, Branco CM. A study on the fatigue behaviour of damaged welded joints repaired by hammer peening. ECF13, San Sebastian, 2000; 2000.
[21] NORSOK Standfard. Material data sheets for structural steel. N-0306 Oslo, Norway: Norway Technology Center; 2000 [Copyright of Advanced Materials Research is the property of Trans Tech Publications].
[22] ESAB, Coreweld C6LF. Available from: https://www.esabna.com/us/en/products/ller-metals/metal-cored-wires-mcaw/mild-steel-wires/coreweld-c6-lf.cfm.
[23] Fricke W. Guideline for the fatigue assessment by notch stress analysis for welded structures. Int Inst Weld 2008;13:2240–308.
[24] Manai A, Franz von Bock und Polach RU, Al-Emrani M. A probabilistic study of welding residual stresses distribution and their contribution to the fatigue life. Eng Fail Anal 2020;118:104787. https://doi.org/10.1016/j.engfailanal.2020.104787.
[25] Brust FW, Kim DS. Mitigating welding residual stress and distortion. In: Processes and mechanisms of welding residual stress and distortion. Woodhead Publishing; 2005. p. 264-94.
[26] Okawa T, Shimanuki H, Nose T, Suzuki T. Fatigue life prediction of welded structures based on crack growth analysis. Nippon Steel Tech Rep 2013;102:51–3.
[27] Kudryavtsev Y, Kleiman J. Ultrasonic technique and equipment for residual stresses measurement. In: Engineering applications of residual stress, vol. 8. New York, NY: Springer; 2011. p. 55–66.
[28] Al-Karawi H, von Bock und Polach RUF, Al-Emrani M. Fatigue crack repair in welded structures via tungsten inert gas remelting and high frequency mechanical impact. J Constr Steel Res 2020;172:106200. https://doi.org/10.1016/j.jcsr.2020.106200.
[29] Al-Karawi H. Fatigue life extension in existing steel bridges [Licentiate dissertation]. Department of Architecture and Civil Engineering, Chalmers University of Technology; 2020.
[30] Anami K, Miki C, Tani H, Yamamoto H. Improving fatigue strength of welded joints by hammer peening and TIG-dressing. Doboku Gakkai Ronbunshu 2000;2000(647):67–78.
[31] Gao W, Wang D, Cheng F, Deng C, Liu Y, Xu W. Enhancement of the fatigue strength of underwater wet welds by grinding and ultrasonic impact treatment. J Mater Process Technol 2015;223:305–12.
[32] Shams-Hakimi P. Fatigue improvement of steel bridges with high-frequency mechanical impact treatment [Doctoral dissertation]. Department of Architecture and Civil Engineering, Chalmers University of Technology; 2020.
[33] Yuan KL, Sumi Y. Modelling of ultrasonic impact treatment (UIT) of welded joints and its effect on fatigue strength. Frattura ed Integrità Strutturale 2015;9(34).
[34] Nitschke-Pagel T, Dilger K, Eslami-Chalandar H. Residual stress determination in mechanically treated weldments with help of different measurement methods.
[35] Liu Y, Wang D, Deng C, Xia L, Huo L, Wang L, et al. Influence of re-ultrasonic impact treatment on fatigue behaviors of S690QL welded joints. Int J Fatigue 2014;66:155–60.
[36] Cheng X, Fisher JW, Prask HJ, Gnäupel-Herold T, Yen BT, Roy S. Residual stress modification by post-weld treatment and its beneficial effect on fatigue strength of welded structures. Int J Fatigue 2003;25(9–11):1259–69.
[37] Ghahremani K, Walbridge S. Fatigue testing and analysis of peened highway bridge welds under in-service variable amplitude loading conditions. Int J Fatigue 2011;33(3):300–12.
[38] Ghahremani K, Walbridge S, Topper T. High cycle fatigue behaviour of impact treated welds under variable amplitude loading conditions. Int J Fatigue 2015;81:128–42.
[39] Tai M, Miki C. Fatigue strength improvement by hammer peening treatment—verification from plastic deformation, residual stress, and fatigue crack propagation rate. Weld World 2014;58(3):307–18.
[40] Al-Emrani M, Shams-Hakimi P, Schneider C, Barsoum Z, Groth H. Fatigue improvement of welded bridge details in stainless steel using High-Frequency Mechanical Impact treatment. In: The ninth international conference on bridge maintenance, safety and management (IABMAS 2018), 9–13 July 2018, Melbourne, Australia. CRC PRESS-Taylor & Francis Group; 2018. p. 446–51.
[41] Fueki R, Takahashi K, Handa M. Fatigue limit improvement and rendering defects harmless by needle peening for high tensile steel welded joint. Metals 2019;9(2):143.
[42] Hellier AK, Prusty BG, Pearce GM, Reid M, Paradowska AM, Simons P. Effect of ultrasonic peening on residual stresses at a T-butt weld toe. Mater Res Proc 2016;2.
[43] Yin D, Wang D, Jing H, Huo L. The effects of ultrasonic peening treatment on the ultra-long life fatigue behavior of welded joints. Mater Des 2010;31(7):3299–307.
[44] British Standards Institution. Guide to methods for assessing the acceptability of flaws in metallic structures. British Standards Institution; 2005.
[45] Hobbacher A. Recommendations for fatigue design of welded joints and components. Cham: Springer International Publishing; 2016.
[46] Drebenstedt K., Euler M. Statistical analysis of fatigue test data according to Eurocode 3. In: Maintenance, safety, risk, management and life-cycle performance of bridges–Proceedings of the ninth international conference on bridge maintenance, safety and management. Melbourne: IABMAS; 2018. p. 2244–51.
[47] E. C. for Standardization. Eurocode 3: Design of steel structures. part 1.9: Fatigue; 2003.
[48] Statnikov ES, Muktepavel VO, Blomqvist A. Comparison of ultrasonic impact treatment (UIT) and other fatigue life improvement methods. Weld World 2002;46(3-4):20–32.
[49] Hui JF, Lloyd JB, Connor RJ. Fatigue life improvement of welded girders with ultrasonic impact treatment. West Lafayette In Purdue University; 2018.
[50] Leitner M, Stoschka M, Eichlseder W. Fatigue enhancement of thin-walled, high-strength steel joints by high-frequency mechanical impact treatment. Weld World 2014;58(1):29–39.
[51] Al-Mukhtar AM. Consideration of the residual stress distributions in fatigue crack growth calculations for assessing welded steel joints. Fatigue Fract Eng Mater Struct 2013;36(12):1352–61.
[52] Al-Mukhtar AM. Residual stresses and stress intensity factor calculations in T-welded joints. J Fail Anal Prev 2013;13(5):619–23.
[53] Ottersböck MJ, Leitner M, Stoschka M. Impact of angular distortion on the fatigue performance of high-strength steel T-joints in as-welded and high frequency mechanical impact-treated condition. Metals 2018;8(5):302.
[54] ISO E. Welding-Fusion-welded joints in steel, nickel, titanium and their alloys (beam welding excluded)—Quality levels for imperfections. ISO 5817: 2014, 2014.